Frontiers in Bioscience Landmark

Front. Biosci. (Landmark Ed) **2023**; 28(8): 169
https://doi.org/10.31083/j.fbl2808169

Original Research

One-Pot Synthesis of Silver Nanoparticles from *Garcinia gummi-gutta*: Characterisation, Antimicrobial, Antioxidant, Anti-Cancerous and Photocatalytic Applications

Jissa Theresa Kurian[1,†], Balamuralikrishnan Balasubramanian[2,†], Arun Meyyazhagan[1], Manikantan Pappuswamy[1], Amer M. Alanazi[3], Kannan RR. Rengasamy[4], Vijaya Anand Arumugam[5,*], Joseph Kadanthottu Sebastian[1,*], Jen-Tsung Chen[6,*]

[1]Department of Life Sciences, CHRIST (Deemed to be University), Bangalore, 560029 Karnataka, India
[2]Department of Food Science and Biotechnology, College of Life Science, Sejong University, 05006 Seoul, Republic of Korea
[3]Pharmaceutical Biotechnology Laboratory, Pharmaceutical Chemistry Department, College of Pharmacy, King Saud University, 11451 Riyadh, Saudi Arabia
[4]Laboratory of Natural Products and Medicinal Chemistry (LNPMC), Department of Pharmacology, Saveetha Dental College, Saveetha Institute of Medical and Technical Sciences (SIMATS), 600077 Chennai, India
[5]Department of Human Genetics and Molecular Biology, Bharathiar University, 641 046 Coimbatore, Tamil Nadu, India
[6]Department of Life Sciences, National University of Kaohsiung, 811 Kaohsiung, Taiwan
*Correspondence: avamiet@yahoo.com (Vijaya Anand Arumugam); joseph.ks@christuniversity.in (Joseph Kadanthottu Sebastian); jentsung@nuk.edu.tw (Jen-Tsung Chen)
[†]These authors contributed equally.
Academic Editor: Graham Pawelec
Submitted: 16 May 2023 Revised: 2 July 2023 Accepted: 20 July 2023 Published: 17 August 2023

Abstract

Background: Methods like the bio-synthesis of silver nanoparticles (Ag NPs) using plant extracts have become promising due to their eco-friendly approach. The study aimed to examine the utilization of *Garcinia gummi-gutta* fruit phytochemicals as agents in the biosynthesis of Ag NPs, evaluation of the antimicrobial, antioxidant, and anti-cancerous properties, as well as the photocatalytic ability of bio-synthesized Ag NPs against Crystal Violet (CV), a triphenylmethane dye. **Methods**: The characterization of the physical properties of the Ag NPs synthesized via the green route was done using UV–Vis spectrophotometry (UV–Vis), X-ray Diffraction (XRD), Fourier Transform Infrared Spectrophotometry (FTIR), Scanning Electron Microscopy (SEM), Zeta potential analysis, and Transmission Electron Microscopy (TEM). The dye degradation efficiency of CV was determined using synthesized Ag NPs under UV light by analyzing the absorption maximum at 579 nm. The antimicrobial efficacy of Ag NPs against *E. coli, S. aureus, Candida tropicalis,* and *Candida albicans* was examined using the broth dilution method. The antioxidant and anti-cancer properties of the synthesized Ag NPs were assessed using the DPPH and MTT assays. **Results**: The UV analysis revealed that the peak of synthesized Ag NPs was 442 nm. Data from FTIR, XRD, Zeta potential, SEM, and TEM analysis confirmed the formation of nanoparticles. The SEM and TEM analysis identified the presence of spherical nanoparticles with an average size of 29.12 nm and 24.18 nm, respectively. Maximum dye degradation efficiency of CV was observed at 90.08% after 320 min without any silver leaching, confirming the photocatalytic activity of Ag NPs. The bio-efficiency of the treatment was assessed using the *Allium cepa* root growth inhibition test, toxicity analysis on *Vigna radiata,* and Brine shrimp lethality assay. **Conclusions**: The findings revealed the environmentally friendly nature of green Ag NPs over physical/chemically synthesized Ag NPs. The synthesized Ag NPs can effectively be used in biomedical and photocatalytic applications.

Keywords: *Garcinia gummi-gutta*; photocatalytic degradation; crystal violet; phytotoxicity; antioxidant; anti-cancer; antimicrobial activity

1. Introduction

Nanotechnology is gaining attention in the fields of material science, biomedicine, and water treatment due to its unique structural and biomedical characteristics, contributing to its widespread applications in different fields of science. The nano-size and composition of these materials influence their electronic, optical, catalytic, and magnetic properties. Metal nanoparticles can be used as potential antimicrobial, antioxidant, anti-inflammatory, anti-cancerous, and photocatalytic agents due to their unique properties [1,2]. Bio-synthesized nanoparticles especially green nanoparticles are the focus of the field due to their non-toxic and eco-friendly nature as compared to the nanoparticles synthesized by chemical and biological methods. The potential applications of green synthesized NPs in the fields of medicine and environmental remediation have been explored by researchers [3–5].

Green-synthesized metal nanoparticles have the potential to be employed as antimicrobial agents against bacteria and fungi. Silver nanoparticles (Ag NPs) synthesized

using *Alocasia indica* leaf extract were reported to have significant antimicrobial activity (99% inhibition) against *S. aureus* bacteria [6]. The study explored the applicability of green Ag NPs in dental implants by investigating the anti-biofilm activity of the NPs [6]. Similarly, various studies have investigated the potential applicability of green synthesized NPs as antimicrobial agents, as well as for biomedical purposes [7,8]. The nanostructure and increased surface area of these materials enable easier penetration of these particles into the microbial cells. Green Ag NPs are significantly effective against multi-drug-resistant bacteria [9].

Ag NPs synthesized from plant extracts can also be used as antioxidant agents due to their potential ability to scavenge free radicals. This property of the green nanoparticles can be effectively used in pharmacognostic applications in modern medicine [10]. The cytotoxic properties of these nanoparticles render them suitable anticancer agents in cancer therapy. Researchers have explored the potential applications of biosynthesized NPs in the treatment of renal cell carcinoma [4]. Biogenic Ag NPs studies revealed improved activity of silver nanoparticles on various cancer cell lines [2].

The modern era of industrialization and urbanization has increased water pollution and one of the major contributors to this pollution is the discharge of dye effluents into water bodies. Crystal Violet (CV) ($C_{25}H_{30}ClN_3$), commonly known as gentian blue is a triphenylmethane dye that is broadly used as a biological stain in human and veterinary medicine. Triphenylmethane dyes including CV are generally used in cosmetics, dyeing, textiles, leather, paper, and food industries [11]. Due to its toxic nature and recalcitrant nature, CV is regarded as a biohazard substance. Studies have revealed its toxic effects on terrestrial, as well as aquatic life. *In vitro* studies on some aquatic organisms have proved that it's a potent mitotic poison and carcinogen, and also promotes tumor growth in fish [12,13]. As the dye is cationic, exposure to it causes painful light sensitization, eye irritations, and cornea injury. Further, CV is considered one of the highly toxic agents to mammalian cells. In extreme situations, CV exposure can lead to respiratory problems and kidney failures [11,14]. Conventional effluent treatment methods are time-consuming, costly, may not be efficient in removing these harmful color molecules, and produce enormous amounts of sludge and poisonous by-products [15]. Hence, the development of a novel, eco-friendly method is essential. Owing to their significant potential for removing new pollutants in aquatic systems, the photocatalytic degradation of textile effluents is the focus of research. Nanomaterials are suitable catalysts as they are highly efficient in degrading high molecular dye compounds without producing toxic by-products [16]. Studies have proved the superior efficiency of metallic NPs in the degradation of textile dyes [17].

Garcinia gummi-gutta, also known as Malabar tamarind, is a member of the Clusiaceae family that is frequently utilized in culinary applications in Western Africa and South East Asia. The fruit contains different phytochemicals such as maleic acid, hydroxy citric acid, tartaric acid, citric acid, phosphoric acid, vitamin C, tartaric acid, and many phenolic compounds. The fruit extracts are used in natural weightless products. It is also used in the treatment of diarrhea, rheumatoid conditions, ulcers, bowel complaints, inflammation, and more [18].

The interest in fruit extract stems from its unexplored applications in various fields such as sustainable nanotechnology and various bio-medicinal applications despite their widespread use in culinary purposes and their easy availability. This knowledge gap generates an opportunity to explore its untapped potential and contribute to the existing scientific understanding. Even though *Garcinia gummi-gutta* fruit extract (GFE) was reported in the synthesis of biogenic Au nanocrystals, its potential in the bioreduction of Ag NPs has received less attention [18,19]. Here, we aim to investigate the possibility of ecologically friendly AgNP synthesis using *Garcinia gummi-gutta* fruit extract.

The antibacterial, anti-cancerous, and antioxidant activities of Ag NPs synthesized from *Garcinia gummi-gutta* fruit extract, as well as their photocatalytic potentials have not yet been investigated. Examining these characteristics can offer useful information on the prospective uses of the synthesized Ag NPs in several industries, including biotechnology, medicine, and environmental remediation.

In this study, Ag NPs were synthesized from silver nitrate using GFE via green synthesis, with plant phytochemicals acting as reducing and capping agents. The synthesized GFE Ag NPs were employed as an antibacterial, antioxidant, anti-cancer, and nano-catalyst in the degradation of CV dye. Utilizing LC-MS analysis, the degraded products were investigated and examined in more detail. We further investigated the bio efficiency of the treatment by testing the toxicity of CV and NP-treated solutions using actual environmental samples.

2. Materials and Methods

2.1 Materials

All chemicals were procured from Hi-media Laboratories Pvt. Ltd. India. Fresh fruits of *Garcinia gummi-gutta* (L.) were procured from fields in Kottayam, India. The dust and impurities were removed by thorough washing. The fruit pericarp and seeds were separated and dried. The dried fruit pericarp was stored at room temperature for further use.

2.2 Plant Extract Preparation and Synthesis of Biogenic Ag NPs

Approximately 10 g of *Garcinia gummi-gutta* dry fruits were suspended in 100 mL of distilled water and subjected to a 1-hour reflux extraction at 40 °C [20]. The

extract was filtered through Whatman No.1 and used for the synthesis of Ag NPs. For the synthesis of Ag NPs, 40 mL 0.01 M $AgNO_3$ solution was mixed with 100 mL GFE and the reaction mixture was refluxed at 60 °C for 30 min. The Ag NPs formation was monitored by a change in the solution color [21]. To remove unreacted precursor/plant particles from the reaction mixture, the GFE Ag NPs were washed at 10,000 rpm for 10 minutes with water followed by ethanol [22].

2.3 Characterization of the Synthesized Ag NPs

Absorption spectra of the GFE Ag NPs were recorded using UV-vis absorption spectroscopic analysis (200-800 nm) (Shimadzu UV-1800ENG240V UV spectrophotometer). FTIR spectra of the plant extract and the GFE Ag NPs were studied using a Shimizu IR sprit with reflectance QATR-S spectrophotometer at a scanning range of 500–4000 cm^{-1} and a resolution of 2 cm^{-1} to identify potential functional groups. The crystal phase information of the synthesized Ag NPs was analyzed using a Rigaku make mini flex X-ray diffractometer operating at 40 kV voltage and 15 mA current with a Cu K-beta ($\times$1.5) radiation monochromatic filter in the range of 5.0–90.0 deg in 2-theta with a scanning speed of 5 deg min^{-1}. The particle size and Zeta potential of GFE Ag NPs were measured using a Malvern zeta sizer ZEN3600 at 25 °C. ZEISS Sigma HV Field Emission Scanning Electron Microscopy (FESEM) was used to examine the surface morphology, shape, and size of the NPs. HRTEM, SAED, and EDS analysis was carried out using Thermofisher Talos F200 S model with FEG, CMOS camera 4K $\times$ 4K operated at 200 KV.

2.4 Antimicrobial Activity of Synthesized Ag NPs

The antibacterial potential of GFE Ag NPs was investigated by determining the Minimum Inhibitory Concentration (MIC) of the NPs against bacterial and fungal strains. The MIC of the GFE Ag NPs was obtained using the broth dilution method validated by Clinical Laboratory Standards Institute. The bacterial strains *E. coli* (ATCC 10536) and *S. aureus* (ATCC 25923), and the fungal strains *Candida tropicalis* (ATCC 10231) *and Candida albicans* (ATCC 90028) were procured from Microbial Type Culture Collection and Gene Bank (MTCC), Institute of Microbial Technology, IMTECH, Chandigarh, India. The active bacterial and fungal cultures were grown in nutrient broth (NB) and Potato Dextrose Broth (PDB), respectively, for 24 hours at 37 °C. The desired concentrations of GFE Ag NPs were prepared by suspending the NPs in sterile distilled water and by sequential dilutions from 300 to 10 $\mu g \cdot mL^{-1}$ in a 48-well Microtiter plate (MTP) containing NB and PDB. The solutions were inoculated with 0.5 mL of microbial culture suspension (1×10^5 cells/mL) and incubated at 37 °C for 24 h. The minimum concentrations of the GFE Ag NPs that inhibited microbial growth were calculated as the MIC values [23,24].

2.5 Antioxidant Activity of GFE Ag NPs

The antioxidant capabilities of the synthesized GFE Ag NPs were evaluated using the previously described method with minor changes [1]. For the study, various concentrations of the NPs (10–60 $\mu g \cdot mL^{-1}$) and ascorbic acid (2–12 $\mu g \cdot mL^{-1}$) solutions were prepared using methanol. A typical reaction system was prepared by adding 10 µL of the sample (ascorbic acid/GFE Ag NPs) to 2000 µL of methanolic DPPH (0.025 mg/mL) and the reaction was carried out for 30 mins in the dark, and 2 mL methanolic DPPH was used as the control system. The absorbance was measured at 517 nm using a UV-vis spectrophotometer [1]. The percentage of DPPH scavenging activity was calculated using the following formula.

$$\text{Percentage of scavenging } (\%) = \left(\frac{A_c - A_T}{A_c}\right) \times 100$$

Where A_c is the absorbance of the control, A_T is the absorbance of the sample.

2.6 MTT Assay

The *in vitro* cytotoxic activity of GFE Ag NPs was analyzed using HEP-G2 cell lines procured from ATCC. The trypsinized monolayer cell culture was adjusted to a cell count of 1.0×10^5 cells/mL by utilizing suitable media containing 10% FBS [25]. The cell lines used in study have been authenticated using Sixteen short tandem repeat (STR) and the tested samples have exhibited 94% match with the ATCC STR profile database. STR loci were amplified using commercially available AmpFISTR Identifier Plus PCR amplification Kit from Biosystems. The cell line sample was processed using the Applied Biosysytems 3500 Genetic analyzer. Data was analysed using Gene mapper ID-X v1.5 software (applied Biosystems, Waltham, MA, USA). Appropriate positive and negative controls were used and confirmed for each sample. The cell lines used are tested for mycoplasma by Hoechst staining/Polymerase Chain Reaction (PCR) method. A 96-well microtiter plate was filled with 100 µL of the diluted cell solution (50,000 cells/well). After 24 hours, a partial monolayer formed, and the supernatant was discarded. The monolayer was rinsed once with media before 100 L of various concentrations (10–100 M) of GFE Ag NPs were added to the wells. The plates were incubated in 5% CO_2 for 24 hours at 37 °C. Further, the Ag NPs solutions in the wells were removed and 100 µL of MTT (5 mg/10 mL of MTT in PBS) was added to each well. After incubating the plate at 37 °C in a 5% CO_2 atmosphere for 4 hours, the supernatant was removed from the wells and 100 µL of DMSO was added. The formazan in the plate was gently shaken to dissolve it, and the absorbance was measured at 590 nm with a microplate reader. Using the formula, the percentage of growth inhibition was calculated.

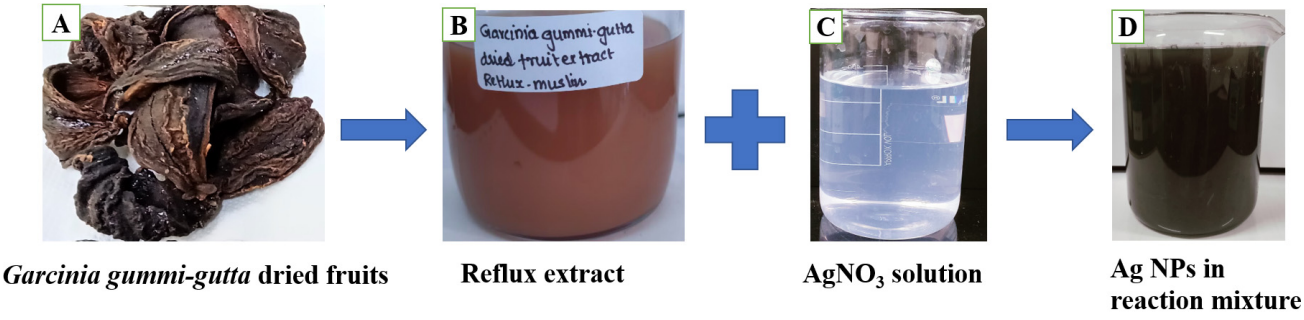

Fig. 1. Schematic representation of the green synthesis of Ag NPs. (A) Dried *Garcinia gummi-gutta* fruit pericarp. (B) Reflux extract of *Garcinia gummi-gutta* fruits. (C) $AgNO_3$ solution. (D) Green synthesized Ag NPs. Ag NPs, silver nanoparticles.

$$\text{Growth inhibition } (\%) = 100 - \left(\frac{\text{OD of the sample}}{\text{OD of the control}} \right) \times 100$$

The concentration of the Ag NPs required to inhibit 50% (IC_{50}) cell growth was calculated from the dose-response curve of the cell line [26].

2.7 Photocatalytic Degradation of Crystal Violet

The photocatalytic degradation ability of Ag NPs was investigated in an aqueous CV solution (0.1 mM) and UV light was used as the light source. NP solution (0.25 mg/mL) was prepared by suspending the synthesized Ag NPs in distilled water by sonicating the solution. CV solution (10 mL) was combined with 20 mL of Ag NPs. The control was a CV solution devoid of NP. The solutions were exposed to UV light for 320 minutes while being constantly stirred. The reaction process was monitored using a UV-vis spectrophotometer by measuring dye absorbance at 10, 20, 40, 80, 160, and 320 min intervals [27]. Degradation efficiency was calculated using the equation.

$$\% \text{ Degradation } = \frac{C_0 - C_t}{C_0} \times 100$$

Where C_0 is the absorbance of the control and C_t is the absorbance of the test sample.

To analyze the degraded products of CV, GFE-NP-treated solution at 320 min was subjected to LC-MS analysis using a Shimadzu LCMS8040 model equipped with a Triple quadrupole analyzer and SPD40- UV-vis detector.

Phytotoxicity Study

Eco-toxicity of the treatment was analyzed by monitoring the toxicity of the untreated CV solution. The reduction in the toxicity of treated dye effluents was also assessed by investigating the *Allium cepa* root growth inhibition test, *Vigna radiata* toxicity study, and by performing the Brine shrimp death experiment. Clean bulbs were grown in distilled water for 72 hours before being subjected to synthesized NP solutions (0.25 mg/mL), test samples (0.1 mM CV solution), and Ag NPs-treated CV dye solutions for 48 hours for the *Allium cepa* root growth inhibition test. As a control, distilled water was used. The root length of the onion bulbs in each solution was measured after exposure, and the percentage of growth inhibition was calculated [28,29]. The seeds of *Vigna radiata* were immersed in distilled water overnight for germination. Each sprout was exposed to test samples including synthesized Ag NPs solutions, CV solution (0.1 mM), and Ag NPs-treated dye solutions. As a control, a seedling was subjected to distilled water. Each sample set was treated with 10 mL sample solutions per day, and the experiment was carried out for 3–4 days. On the 4th day, the *Vigna radiata* seedlings were harvested and the length of the leaf and stem root, and the total length of the seedling were measured, subsequently, the percentage of leaf, stem, and root growth inhibition was calculated [27,28]. The brine shrimp lethality experiment was used to examine the treatment efficacy as a quick technique for analyzing the cytotoxic effects of synthesized Ag NPs, and treated and untreated dye solutions. The Brine prawn, *Artemia salina* (L), was nurtured in the same manner as previously described [30]. After 48 hours, matured nauplii were used for analysis. For the toxicity analysis, 5 mL of artificial seawater mixed with 5 mL of a test solution (synthesized Ag NPs, untreated or treated CV dye) was collected in test tubes and 10 mL of artificial seawater was kept as the control for the assay. A total of 30 matured nauplii were introduced to each of the samples (both the test samples and the control samples). For 24 hours, the setup was left uncovered under a constant light source. The number of surviving shrimps and dead nauplii was counted after 24 hours of exposure, and the percentage of mortality was computed [29].

3. Results and Discussion

3.1 Synthesis of Ag NPs Using Garcinia gummi-gutta Fruit Extract

The presence of phytochemicals such as flavonoids, alkaloids, and many other phytochemicals in *Garcinia gummi-gutta* extracts has been observed in phytochemical investigations [31]. During the reduction reaction, these

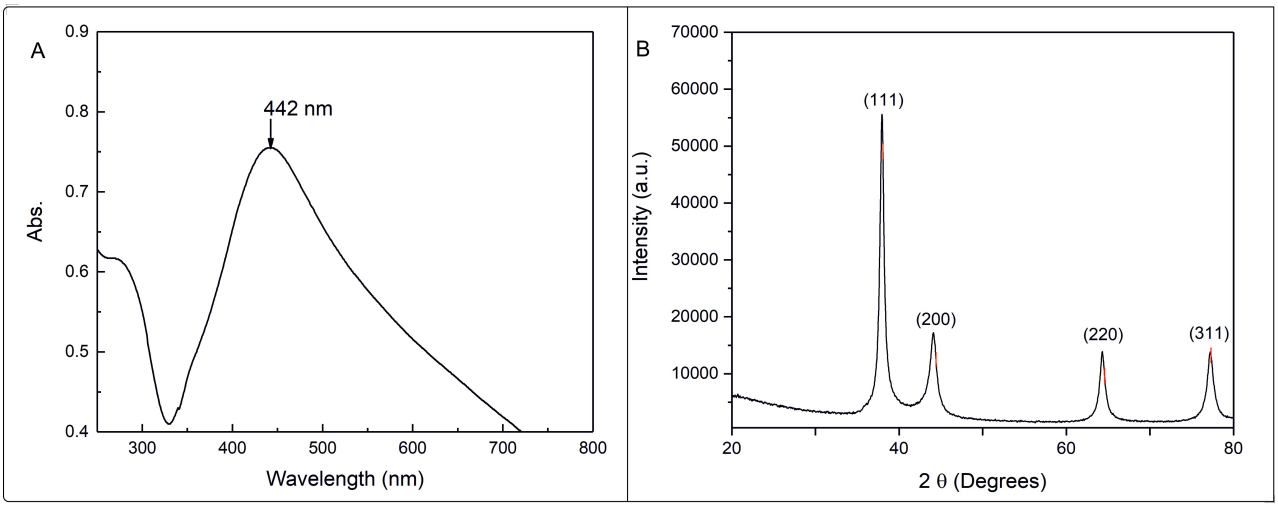

Fig. 2. (A) Spectrum showing the SPR peak, and (B) XRD pattern of Ag NPs synthesized from GFE. SPR, Surface Plasmon Resonance; GFE, *Garcinia gummi-gutta* fruit extract; XRD, X-ray Diffraction.

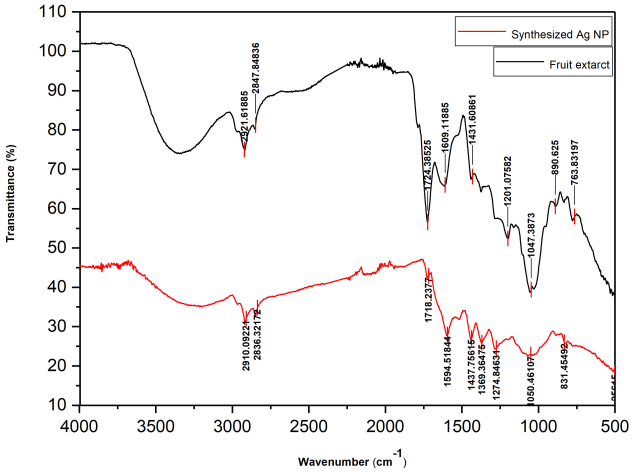

Fig. 3. Fourier Transform Infrared Spectrophotometry (FTIR) of the *Garcinia gummi-gutta* fruits extract and the synthesized Ag NPs.

phytochemicals act as reducing and capping agents in the synthesis of Ag NPs. The initial yellow color in the reaction mixture turned brownish-black, indicating the synthesis of Ag NPs in the mixture. The presence of a large number of phytochemicals in the plant extract that acted as reducing and capping agents in the production of Ag NPs was confirmed by the color change observed within 20 minutes of the reaction. After 30 minutes of reaction, the color of the reaction mixture changed to brownish black, indicating that the Ag NPs in the reaction mixture had been fully reduced. The reaction mixture was further examined to confirm the production of Ag NPs (Fig. 1). Similar observation was seen using banana peel extracts [21].

3.2 Characterization of GFE Ag NPs

UV-vis spectrophotometry was used to confirm the production of Ag NPs in the reaction mixture after the GFE Ag NPs were synthesized. In the UV-vis absorption spectra of pure Ag NPs, a surface plasmon resonance (SPR) peak at 442 nm was identified, confirming its formation (Fig. 2A). The GFE and green synthesized Ag NPs were analyzed using FTIR to identify potential biomolecules involved in Ag NP synthesis. The acquired spectrum revealed several distinct peaks that confirm and support the generation of Ag NPs and the role of plant phytochemicals in Ag NP synthesis.

The resulting FTIR spectra of GFE showed peaks at 2921.61 (cm^{-1}) and 2847.84 (cm^{-1}) that represent the C-H stretching of alkanes, 1724.38 (cm^{-1}) and 1431.60 (cm^{-1}) that are associated with the C=O stretching carboxylic acid dimer O-H bending carboxylic acid, 1201.07 (cm^{-1}) that indicates the C-O stretching alkyl aryl ether in the extract, and 1047.38 (cm^{-1}) and 890.62 (cm^{-1}) that are due to CO-O-CO stretching of anhydride and C=C bending of alkene vinylidene, respectively, indicating the presence of phenols, flavonoids, and anthocyanins in abundance [14]. On the other hand, the FTIR spectra of Ag NPs synthesized from GFE showed characteristic peaks at 2910.92, 2836.32, 1718.23, 1594.51, 1437.75, 1369.36, 1274.84, 1050.46 and 831.45 (cm^{-1}) representing C-H stretching alkane, C=O stretching of the carboxylic acid dimer, N-H bending due to the amine group, O-H bending of carboxylic acid, N-O stretching of the nitro compound, C-O stretching of the alkyl aryl ether, CO-O-CO stretching of anhydride groups, and C=C bending of alkene, respectively (Fig. 3). The band at 1724.38 (cm^{-1}) that represents C=O stretching of the carboxylic acid dimer is likely due to the presence of hydroxy citric acid, the major organic acid found in GFE, as the carboxyl group is the characteristic group of hydroxy citric

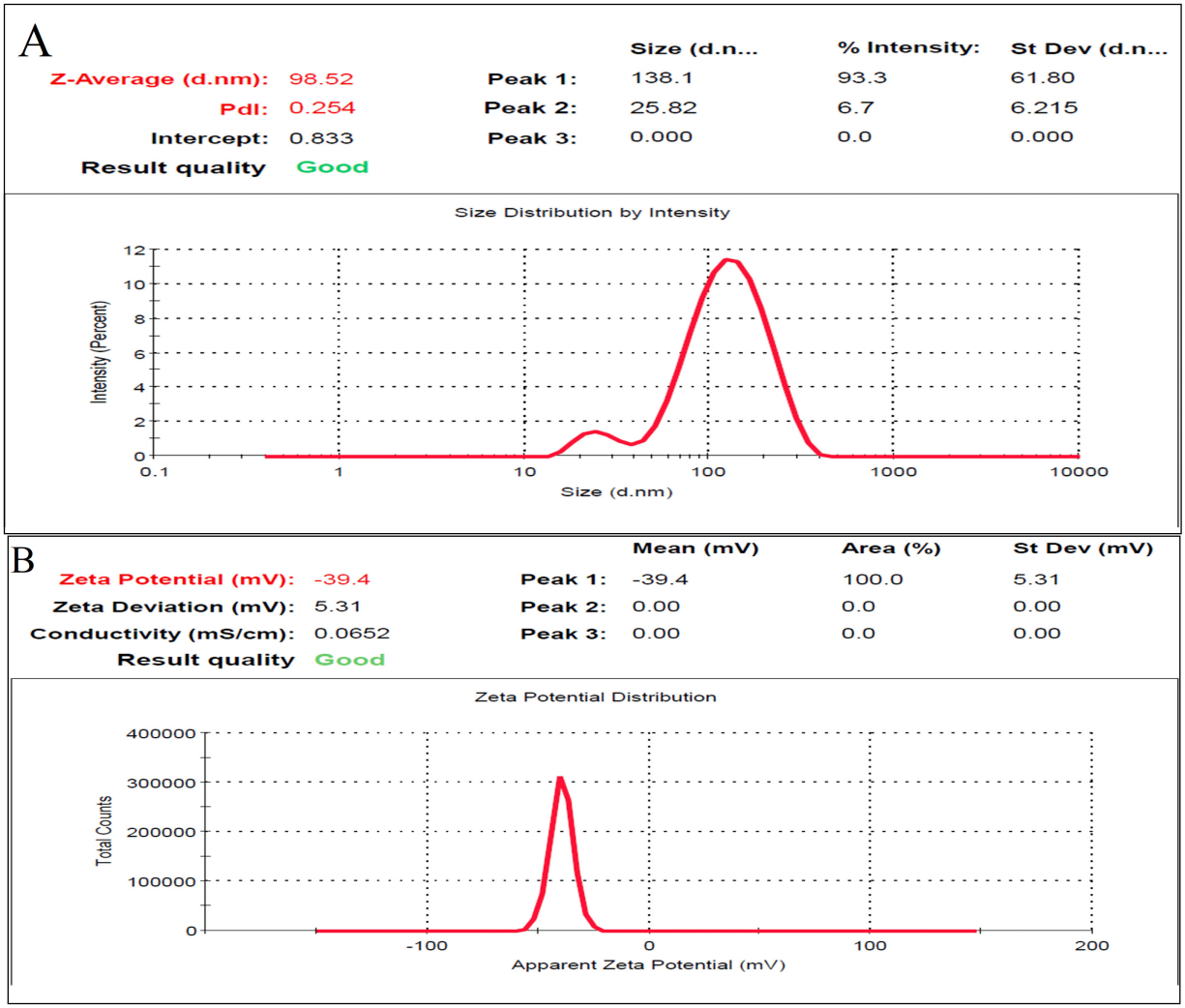

Fig. 4. Dynamic Light Scattering (DLS) analysis of the green synthesized Ag NPs. (A) Particle size analysis of the green synthesized Ag NPs. (B) Zeta potential analysis of the green synthesized Ag NPs.

acid [32]. The GFE spectra revealed a significant decrease in the intensity of the band at 1718.23 (cm^{-1}) indicating the effective involvement of the carboxylic acid group in the bioreduction of Ag^{+} ions to nanoparticles [18].

The crystalline phase of the synthesized GFE Ag NPs was obtained by X-ray Diffraction (XRD) analysis. XRD spectrum of the synthesized Ag NPs revealed the characteristic peaks of Ag NPs with 2-theta values, 38.06^{0}, 44.39^{0}, 64.57^{0}, and 77.28^{0} corresponding to [111], [200], [220], and [311] sets of lattice planes, respectively, by JCPDS file no: 89-3722 [33]. These planes can be indexed as the band of face-centered cubic structures of Ag NPs. XRD spectrum of the synthesized Ag NPs suggests the crystalline nature of the Ag NPs synthesized using GFE. Similar results were reported for Ag NPs from *Jatropha curcas* [34]. Using Debye-Scherrer's equation, $D = 0.9\lambda/\beta \cos\theta$, the average crystallite size of the synthesized Ag NPs was calculated to be 11.06 nm [35], where, D is the average crystallite size, λ is the wavelength of the X-Ray used, β is the full length at half maximum, and θ is Bragg's diffraction angle (Fig. 2B).

The synthesized Ag NPs were subjected to Dynamic Light Scattering (DLS) analysis to monitor the fluctuations in the light intensity of the synthesized NPs [36]. The study found particles of two distinct sizes, which could be attributed to the agglomeration of the synthesized NPs (Fig. 4A). The synthesized Ag NPs had an average particle size of 98.52 nm. The charge distribution of the synthesized Ag NPs was confirmed by zeta potential analysis. The observed zeta potential value of the synthesized Ag NPs (-39.4 ± 5.31 mV) suggests the stability of the green synthesized Ag NPs (Fig. 4B). The surface phase analysis of the synthesized Ag NPs was performed using FESEM analysis. The FESEM images show the spherical morphology and agglomeration of the synthesized Ag NPs with an average size of 29.12 nm due to electrostatic attraction and polarity (Fig. 5A). Agglomeration of NPs was also reported in *Garcinia mangostana* [20].

The TEM analysis of the synthesized GFE Ag NPs was performed to better analyze the surface characteristics and the crystalline nature of the NPs (Fig. 5B). TEM

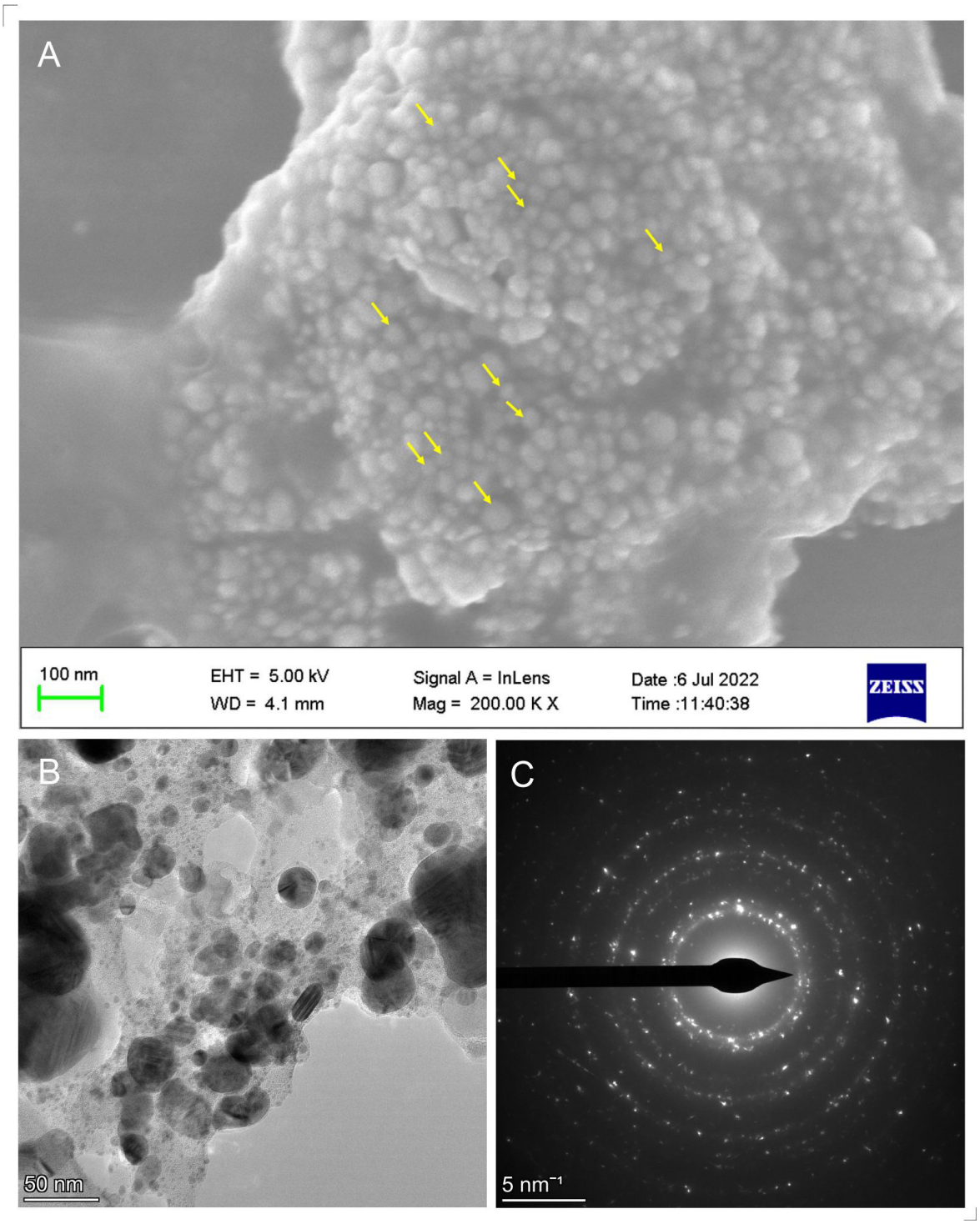

Fig. 5. Field emission scanning electron microscopy (FE-SEM) (A), High-resolution transmission electron microscopy (HRTEM) images (B) with Selected area electron diffraction (SAED) patterns (C) of green synthesized Ag NPs.

scans revealed spherical-shaped particles averaging 24.18 nm in size. The SAED patterns of the GFE Ag NPs revealed concentric rings, confirming the crystalline structure of the NPs. According to XRD examination, the d-spacing values of SAED patterns were 0.244, 0.208, 0.146, and 0.123 nm, corresponding to the [111], [200], [220], and [311] planes of Face centered cubic planes, respectively (Fig. 5C) [2]. EDS tests were used to determine the elemental composition of the GFE Ag NPs, revealing very intense silver peaks followed by carbon and oxygen (Fig. 6). The presence of carbon and oxygen can be attributed to bioactive substances such as flavonoids, phenols, and alkaloids that function as capping agents on the surface of biogenic Ag NPs [2].

Table 1. Minimum inhibitory concentration of GFE Ag NPs against different microbial strains.

Microorganism	Microbial strains	IC_{90} (µg·mL^{-1})	MIC (µg·mL^{-1})	Percentage of inhibition at MIC (%)
Bacteria	*E. coli*	30.26	100	96.69
	S. aureus	50.84	100	96.59
Fungi	*Candida albicans*	87.16	100	94.05
	Candida tropicalis	50.79	100	95.11

MIC, Minimum Inhibitory Concentration.

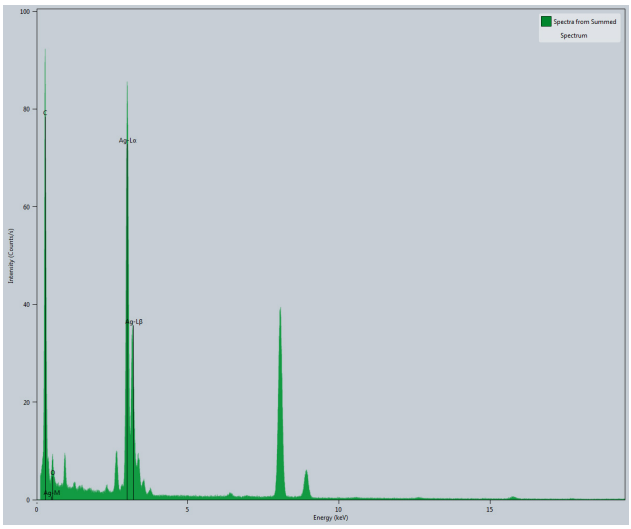

Fig. 6. The Energy Dispersive X-ray (EDX) spectrum of the synthesized Ag NPs.

3.3 Antimicrobial Activity of Synthesized Ag NPs

To evaluate the antimicrobial properties of the synthesized GFE Ag NPs against bacterial strains, *E. coli* (ATCC 10536) and *S. aureus* (ATCC 25923), and the fungal strains, *Candida tropicalis* (ATCC 10231) and *Candida albicans* (ATCC90028), the MIC analysis was performed with GFE Ag NPs at varying concentrations (20–100 µg·mL^{-1}). The GFE Ag NPs showed potential antibacterial activity against *E. coli* (ATCC 10536) and *S. aureus* (ATCC 25923) with an IC_{90} of 30.26 µg·mL^{-1} and 50.84 µg·mL^{-1}, respectively (Table 1). GFE Ag NPs displayed significant antifungal activities against *Candida tropicalis* (ATCC 10231) and *Candida albicans* (ATCC 90028) with an IC_{90} of 50.79 µg·mL^{-1} and 87.16 µg·mL^{-1}, respectively. The highest activity was observed against *E. coli* and the least was on *Candida albicans*. The synthesized NPs display more activity against bacterial strains than the fungal strains. This may be due to the difference in their cell structures and the cell membrane compositions. Early studies have reported the improved antimicrobial activity of the green synthesized NPs compared to NPs synthesized by other methods [1]. The results show that Gram-negative bacteria were more vulnerable to GFE Ag NPs than Gram-positive bacteria, possibly due to differences in cell wall composition, as previously described [1].

3.4 Antioxidant Activity of the GFE Ag NPs — DPPH Assay

Antioxidants are substances that may scavenge free radicals, thus protecting cells from harmful effects of reactive oxygen species created in cells. Antioxidants are important characteristics that maintain the balance between oxidants and antioxidants and thereby control the defense mechanism of the body [37]. DPPH is a free radical with a purple color, possessing absorption maxima at 517 nm and becomes yellow color upon neutralization of the free radicals. The antioxidant Ag NPs donate electrons or protons to the DPPH radicals, reducing those radicals that subsequently leads to a reduction in the color intensity, and thereby a reduced absorbance. Varying concentration of ascorbic acid (2–12 µg·mL^{-1}) was used as the standard for the assay which exhibited 83.5% (12 µg·mL^{-1}) scavenging activity with an IC_{50} 7.51 µg·mL^{-1}. The GFE Ag NPs also exhibited good antioxidant properties. Furthermore, 60 µg·mL^{-1} of the synthesized Ag NPs have produced 78.6 % DPPH scavenging with an IC_{50} of 41.2 µg·mL^{-1}.

3.5 MTT Assay

The GFE Ag NPs were tested for anti-cancer activity against HEP-G2 hepatic cancer cell lines. The cytotoxic activity of GFE Ag NPs at various concentrations (10–100 M) was tested *in vitro* using the MTT assay (Fig. 7). Higher cytotoxic activity of HEP-G2 cell lines was observed with increasing concentrations of GFE Ag NPs (Fig. 7E). The IC_{50} of the GFE Ag NPs was calculated as 44.75 $\pm$ 0.05 µM. HEP-G2 cell lines treated with GFE Ag NPs exhibited cell deformities such as cell ruptures and shape deformations, while the control cells remain uninterrupted with intact oval shape (Fig. 7A–D). The GFE Ag NPs showed significantly lower effects on the normal hepatic cells, however, cytotoxicity and anticancer assays using these nanoparticles need to be extensively carried out using *in vitro* and *in vivo* methods. The effects on the anti-cancerous activities of GFE Ag NPs may be associated with the phytochemicals that aid in the synthesis of Ag NPs. The major compounds present in *Garcinia* extract — Garcinol, and Hydroxy citric acid are proven to have anti-inflammatory, cytotoxic, and cell apoptosis regulatory properties [38,39].

3.6 Photocatalytic Degradation of CV Dye

The photocatalytic performance of the synthesized Ag NPs was investigated by using the synthesized Ag NPs

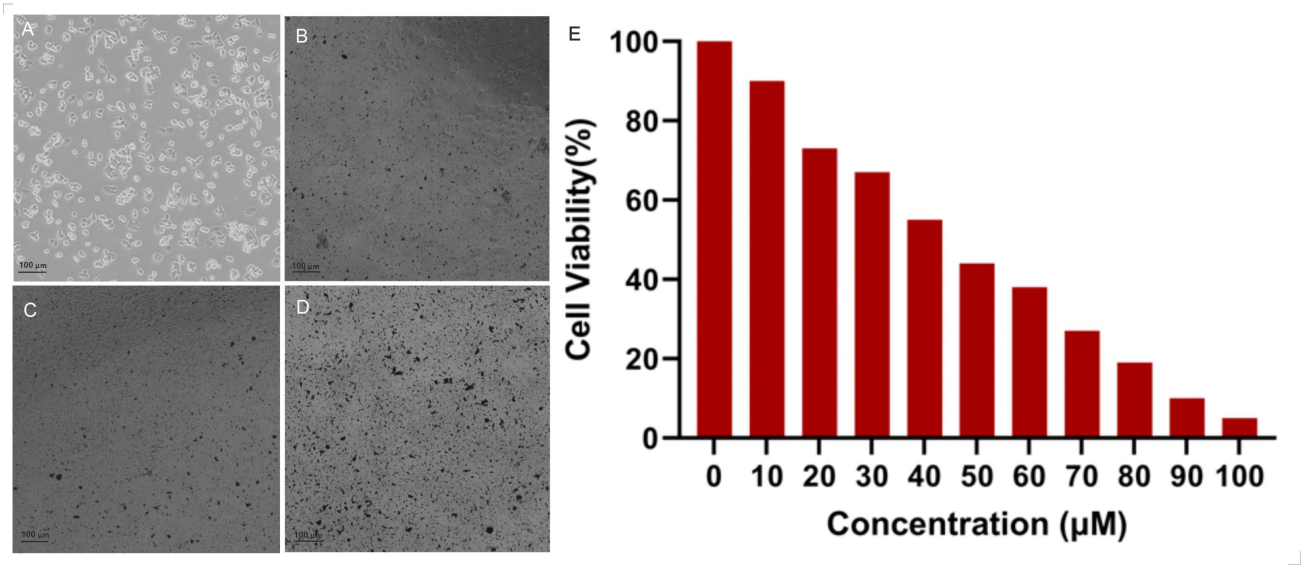

Fig. 7. Cytotoxic potential of synthesized Ag NPs on HEP-G2 cell lines. (A) HEP-G2 control cell lines (B), (C), (D) HEP-G2 cell lines treated with synthesized Ag NPs (100 µM). (E) Graphical representation of reduction in cell viability of HEP-G2 cell lines with different concentrations of Ag NPs.

to degrade CV dye. The absorption maxima of CV were recorded at 579 nm using the UV-vis Spectrophotometer. The absorption spectra revealed decreasing peaks at various time intervals (Table 2). After 320 minutes, the percentage degradation efficiency was calculated to be 90.08% of UV irradiation (Figs. 8,9). Smaller-sized NPs due to their larger surface area significantly increase the rate of photocatalytic degradation. Since it may increase the number of the coordinate atoms, mediating adsorbed dyes could enhance photocatalytic degradation [40,41].

Table 2. Absorbance data of CV degradation with respect to time.

Time interval	Absorbance at 579 nm
control	0.452
00 min	0.197
10 min	0.167
20 min	0.155
40 min	0.128
80 min	0.127
160 min	0.080
320 min	0.043

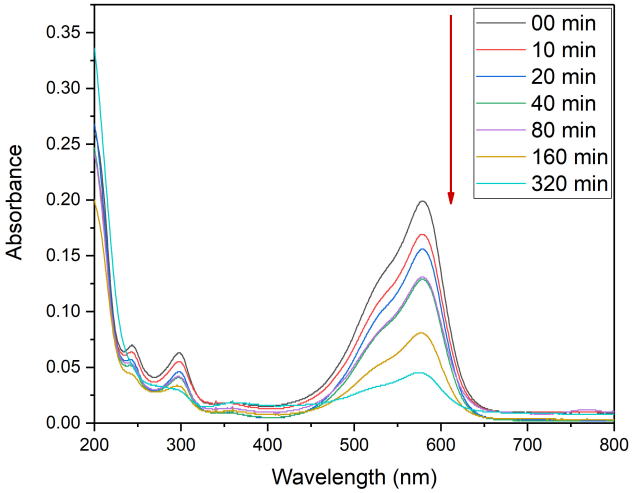

Fig. 8. Photocatalytic degradation of Crystal Violet using green synthesized Ag NPs.

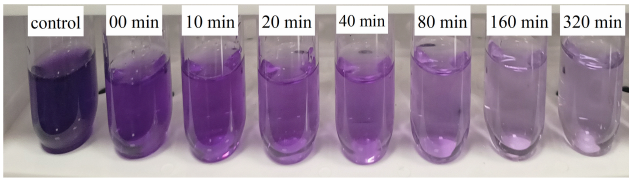

Fig. 9. Image depicting the degradation of Crystal Violet at different time intervals.

3.7 LC-MS Analysis of the Degraded Products.

The effectiveness of CV degradation is determined by the identification of the degraded products, which provides a better understanding of the photocatalytic degradative mechanism. In the present study, degraded products generated during the photocatalytic degradation reaction was examined using LC-MS analysis of the NP-treated CV solution at the point of completion of the reaction. The resulting chromatogram showed a notable intensity difference between the control and the treated CV solution, indicating that CV was effectively degraded (Fig. 10A). Seven sep-

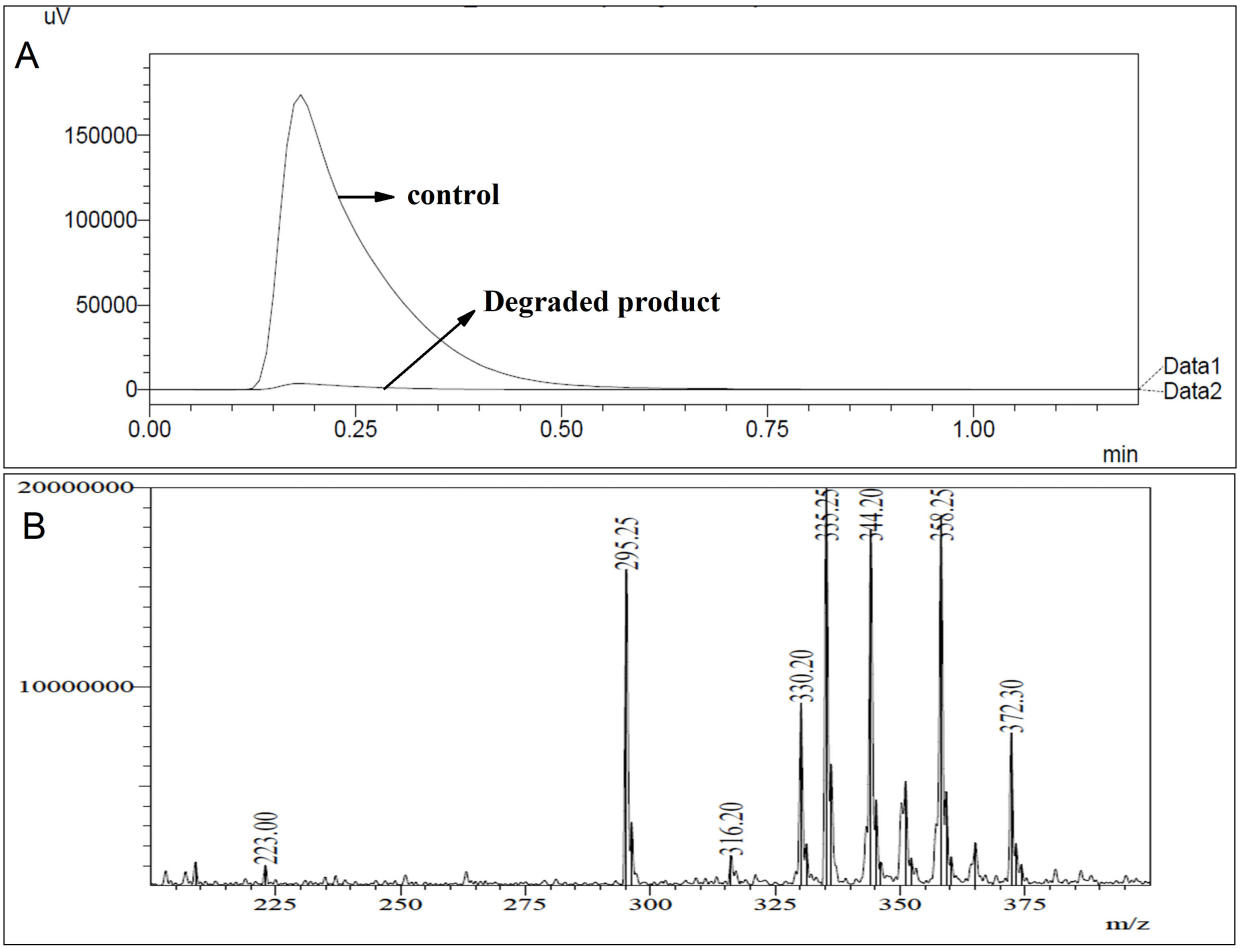

Fig. 10. LC-MS analysis of the degraded products. (A) chromatogram comparison of control CV and the NP-treated dye solution. (B) Mass spectra of N-demethylated products of CV from the CV degradation.

Table 3. Phytotoxicity studies on the degraded CV dye using green synthesised Ag NPs.

Conditions	*Allium cepa* toxicity		*Vigna radiata* toxicity			Brine shrimp lethality
	Root growth inhibition (%)	Leaf toxicity (%)	Stem toxicity (%)	Root toxicity (%)	Total growth inhibition (%)	Mortality (%)
Distilled water	0.00 ± 0.00	0.00 ± 0.00	0.00 ± 0.00	0.00 ± 0.00	0.00 ± 0.00	2.67 ± 2.31
CV control	52.70 ± 2.46	24.33 ± 2.15	38.93 ± 0.31	46.50 ± 0.49	22.89 ± 0.67	100.00 ± 0.00
Synthesized Ag NP	18.71 ± 0.27	7.07 ± 0.72	7.84 ± 0.52	24.81 ± 0.49	9.66 ± 0.39	4.11 ± 0.71
Test - treated	22.00 ± 2.18	8.08 ± 0.72	7.33 ± 0.62	32.51 ± 0.49	10.59 ± 0.62	22.69 ± 2.52

arate m/z peaks were identified (Fig. 10B). These peaks were, in order, 372.3, 358.3, 344.2, 330.3, 316.4, 302.2, and 288.1. The components m/z 372.3 represent the parent molecules that are CV in their ionised form. And the remaining components m/z 358.2, 344.2, 335.2, 330.20, 316.4, and 295.2 were parent CV, mono-, di-, tri-, tetra-, penta-, and hexa-N-de-methylated intermediates, respectively (Fig. 11). Similar results were observed by He *et al.* [42] in a microwave-assisted catalytic degradation of CV by nickel dioxide nanosuspensions.

The N-demethylation of CV occurred gradually, as observed according to the degraded products identified by LC-MS analysis. The presence of some isomeric intermediates was identified from the LC-MS spectra. There were two isomeric intermediates for the di-N-de-methylated product, three for the tri-N-de-methylated product, and two for the tetra-N-de-methylated product (Fig. 11). De-methylation and the destruction of the conjugated ring structures are the two main ways that CV degrades [42]. The photocatalytic activity of the green synthesized GFE-Ag NPs was used in the present study to describe the degradation of CV through de-methylation of the dye molecules.

3.8 Phytotoxicity Study

Wastewater containing dye effluents released into land or water bodies can have significant effects on soil fertil-

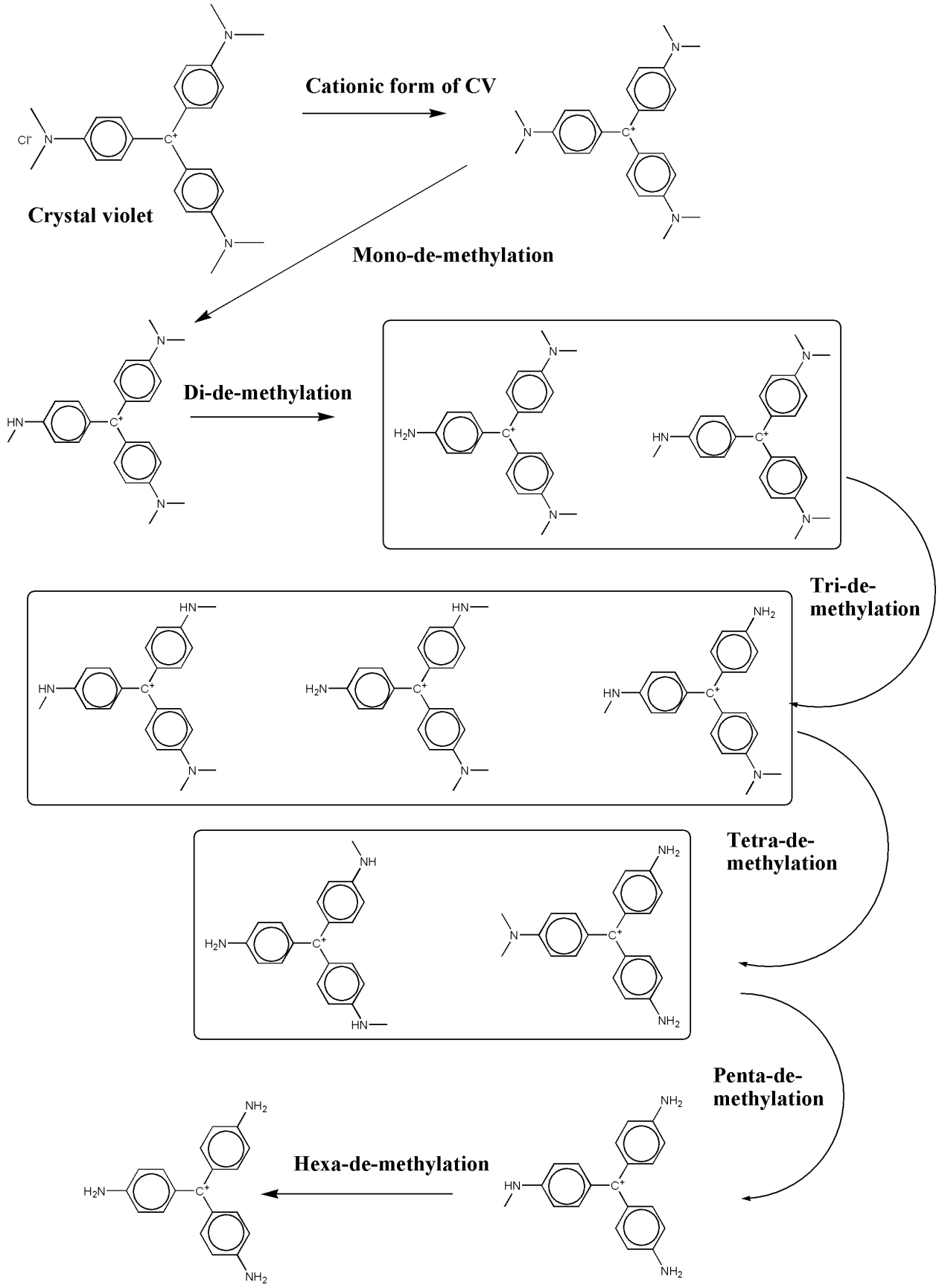

Fig. 11. UV-mediated photocatalytic degradation mechanism of CV by GFE Ag NPs.

ity and organisms at different tropic levels. Hence the release of treated (degradation products) and untreated dyes should be monitored to reduce toxicicity or making it non-toxic for living organisms. An *Allium cepa* root growth inhibition test was carried out to analyze the bio-efficiency of the treatment. Onions treated with CV dye before the treatment with NPs have been shown to exhibit 52.70% inhibition on onion root growth. This was reduced to 22.00% for the samples that were exposed to dye solutions treated with Ag NPs synthesized from GFE (Table 3). Similarly, the effect of treated and untreated solutions dye solutions on *V. radiata* was monitored for the growth inhibition % of the leaf, stem, and root of the green gram sprouts. CV solution before treatment with NPs retarded the growth of the green gram sprouts, and the samples exposed to AgNP-treated solutions have shown normal growth similar to the control samples. The Brine shrimp (*Artemia salina*) toxicity analysis was carried out based on the mortality % of the dye solutions before and after treatment with NPs. All the Brine shrimp nauplii exposed to untreated CV solutions died within 24 h of incubation, indicating the severe toxicity of CV on brine shrimp growth. The mortality rate of the brine shrimp nauplii exposed to dye solutions that were treated with green synthesized Ag NPs was reduced to 20–25%, depicting the efficient degradation of dye compounds in the solution by the green synthesized Ag NPs (Table 3).

4. Conclusions

The GFE Ag NPs were characterized using several spectroscopic and microscopic investigations. The SEM examination revealed spherical-shaped NPs with an average size of 29.12 nm. Similar results were observed during TEM analysis. The GFE Ag NPs were proven to have good antimicrobial, antioxidant, and anti-cancerous activities. This study investigated the photocatalytic capability of Ag NPs in the breakdown of CV dye. Phytotoxicity studies of the Ag NP-treated products revealed significant toxicity reduction of dye and its degraded products. The current study uses renewable and eco-friendly methods for Ag NP synthesis and its biological and catalytic properties. This methodology can be used alone or used with a hybrid system for the efficient removal of dye molecules from textile effluents.

Availability of Data and Materials

The data presented in this study are available on request from the corresponding authors.

Author Contributions

This research article was produced through collaboration between the authors. Conceptualization, VAA, BB, and JKS; Writing the original manuscript, JTK, and BB; Methodology, data curation, and formal analysis, JTK, AM, KRRR, MP, AMA, J-TC; Review and editing, BB, VAA, AMA, KRRR, J-TC; Interpretation, and review/revision, AM, VAA, KRRR, and JKS. All authors contributed to editorial changes in the manuscript. All authors read and approved the final manuscript. All authors have participated sufficiently in the work and agreed to be accountable for all aspects of the work.

Ethics Approval and Consent to Participate

Not Applicable.

Acknowledgment

All the authors are thankful to their respective Universities and Institutes for their support. The authors are thankful to Common Instrumentation Lab, Materials Research Lab-Department of Physics, CHRIST (Deemed to be University) for providing the instrumentation facilities and Major Research Project (MRP DSC-1830, MRP DC-1934), Centre for Research, CHRIST (Deemed to be University) for providing the DLS analysis facilities. We also thank the Department of Physics, Cochin University of Science and Technology for providing the SEM analysis facilities. The authors acknowledge the Central Research Facilities, Centre for Nano and Soft Matter Sciences, Bengaluru for providing TEM facilities and this work was funded by the Researchers Supporting Project Number (Project Number: RSP2023R261) King Saud University, Riyadh, Saudi Arabia.

Funding

This research received no external funding.

Conflict of Interest

Given the role as Guest Editor and Editorial Member, Jen-Tsung Chen had no involvement in the peer-review of this article and has no access to information regarding its peer-review. Full responsibility for the editorial process for this article was delegated to Graham Pawelec. The authors declare no conflict of interest.

References

[1] Wang L, Wu Y, Xie J, Wu S, Wu Z. Characterization, antioxidant and antimicrobial activities of green synthesized silver nanoparticles from Psidium guajava L. leaf aqueous extracts. Materials Science & Engineering. C, Materials for Biological Applications. 2018; 86: 1–8.

[2] Anandan M, Poorani G, Boomi P, Varunkumar K, Anand K, Chuturgoon AA, *et al*. Green synthesis of anisotropic silver nanoparticles from the aqueous leaf extract of Dodonaea viscosa with their antibacterial and anticancer activities. Process Biochemistry. 2019; 80: 80–88.

[3] Kurian JT, Chandran P, Sebastian JK. Synthesis of Inorganic Nanoparticles Using Traditionally Used Indian Medicinal Plants. Journal of Cluster Science. 2022; 1–27.

[4] Hossain N, Chowdhury MA, Kchaou M, Alam A, Rahman MM. Scope of Bio-based nanoparticle targeted through the cancer zone to deactivate cancer affected cells. Chemical Physics Impact. 2023; 100180.

[5] Rahman A, Chowdhury MA, Hossain N. Green synthesis of hybrid nanoparticles for biomedical applications: A review. Applied Surface Science Advances. 2022; 11: 100296.
[6] Hossain N, Islam MA, Chowdhury MA. Synthesis and characterization of plant extracted silver nanoparticles and advances in dental implant applications. Heliyon. 2022; 8: e12313.
[7] Hossain N, Islam MA, Chowdhury MA, Alam A. Advances of nanoparticles employment in dental implant applications. Applied Surface Science Advances. 2022; 12: 100341.
[8] Hossain N, Chowdhury MA, Hossain A, Ahmed MS, Rana MM, Sultana S. Synthesis and Characterization of Alocasia indica Infused Silver Nanoparticles for Dental Implant Applications. Chemical Physics Impact. 2023; 100239.
[9] Lokina S, Stephen A, Kaviyarasan V, Arulvasu C, Narayanan V. Cytotoxicity and antimicrobial activities of green synthesized silver nanoparticles. European Journal of Medicinal Chemistry. 2014; 76: 256–263.
[10] Sreelekha E, George B, Shyam A, Sajina N, Mathew B. A comparative study on the synthesis, characterization, and antioxidant activity of green and chemically synthesized silver nanoparticles. BioNanoScience. 2012;11: 489–496.
[11] Mani S, Bharagava RN. Exposure to Crystal Violet, Its Toxic, Genotoxic and Carcinogenic Effects on Environment and Its Degradation and Detoxification for Environmental Safety. Reviews of Environmental Contamination and Toxicology. 2016; 237: 71–104.
[12] Au W, Pathak S, Collie CJ, Hsu TC. Cytogenetic toxicity of gentian violet and crystal violet on mammalian cells *in vitro*. Mutation Research. 1978; 58: 269–276.
[13] Fan HJ, Huang ST, Chung WH, Jan JL, Lin WY, Chen CC. Degradation pathways of crystal violet by Fenton and Fenton-like systems: condition optimization and intermediate separation and identification. Journal of Hazardous Materials. 2009; 171: 1032–1044.
[14] Ahmad R. Studies on adsorption of crystal violet dye from aqueous solution onto coniferous pinus bark powder (CPBP). Journal of Hazardous Materials. 2009; 171: 767–773.
[15] Nagajyothi PC, Prabhakar Vattikuti SV, Devarayapalli KC, Yoo K, Shim J, Sreekanth TVM. Green synthesis: Photocatalytic degradation of textile dyes using metal and metal oxide nanoparticles-latest trends and advancements. Critical Reviews in Environmental Science and Technology. 2020; 50: 2617–2723.
[16] Luque PA, Chinchillas-Chinchillas MJ, Nava O, Lugo-Medina E, Martínez-Rosas ME, Carrillo-Castillo A, *et al*. Green synthesis of tin dioxide nanoparticles using Camellia sinensis and its application in photocatalytic degradation of textile dyes. Optik. 2021; 229: 166259.
[17] Chand K, Cao D, Fouad DE, Shah AH, Dayo AQ, Zhu K, *et al*. Green synthesis, characterization and photocatalytic application of silver nanoparticles synthesized by various plant extracts. Arabian Journal of Chemistry. 2020; 13: 8248–8261.
[18] Rajan A, MeenaKumari M, Philip D. Shape tailored green synthesis and catalytic properties of gold nanocrystals. Spectrochimica Acta. Part A, Molecular and Biomolecular Spectroscopy. 2014; 118: 793–799.
[19] Sarip NA, Aminudin NI, Danial WH. Green synthesis of metal nanoparticles using Garcinia extracts: a review. Environmental Chemistry Letters. 2022; 20: 469–493.
[20] Aminuzzaman M, Ying LP, Goh W-S, Watanabe A. Green synthesis of zinc oxide nanoparticles using aqueous extract of Garcinia mangostana fruit pericarp and their photocatalytic activity. Bulletin of Materials Science. 2018; 41: 50.
[21] Ibrahim HM. Green synthesis and characterization of silver nanoparticles using banana peel extract and their antimicrobial activity against representative microorganisms. Journal of Radiation Research and Applied Sciences. 2015; 8: 265–275.
[22] Wang C, Kim YJ, Singh P, Mathiyalagan R, Jin Y, Yang DC. Green synthesis of silver nanoparticles by Bacillus methylotrophicus, and their antimicrobial activity. Artificial Cells, Nanomedicine, and Biotechnology. 2016; 44: 1127–1132.
[23] Balouiri M, Sadiki M, Ibnsouda SK. Methods for *in vitro* evaluating antimicrobial activity: A review. Journal of Pharmaceutical Analysis. 2016; 6: 71–79.
[24] Gonelimali FD, Lin J, Miao W, Xuan J, Charles F, Chen M, *et al*. Antimicrobial Properties and Mechanism of Action of Some Plant Extracts Against Food Pathogens and Spoilage Microorganisms. Frontiers in Microbiology. 2018; 9: 1639.
[25] Frei M. Cell viability and proliferation. Sigmaaldrich tech-Doc BioFiles Online. 2011; 6: 17–21.
[26] Denizot F, Lang R. Rapid colorimetric assay for cell growth and survival. Modifications to the tetrazolium dye procedure giving improved sensitivity and reliability. Journal of Immunological Methods. 1986; 89: 271–277.
[27] Jishma P, Roshmi T, Snigdha S, Radhakrishnan EK. Kinetic study of gold nanoparticle mediated photocatalytic degradation of Victoria blue. 3 Biotech. 2018; 8: 97.
[28] Bilal M, Iqbal M, Hu H, Zhang X. Mutagenicity, cytotoxicity and phytotoxicity evaluation of biodegraded textile effluent by fungal ligninolytic enzymes. Water Science and Technology: a Journal of the International Association on Water Pollution Research. 2016; 73: 2332–2344.
[29] Doshi GM, Kanade PP. Evaluation of bioactivity of *Cucurbita pepo* L., *Cucumis melo* L. and *Cucumis sativus* L. seed extracts. Indian Journal of Experimental Biology. 2019; 57: 269–273.
[30] Supraja N, Prasad TNVKV, Gandhi AD, Anbumani D, Kavitha P, Babujanarthanam R. Synthesis, characterization and evaluation of antimicrobial efficacy and brine shrimp lethality assay of *Alstonia scholaris* stem bark extract mediated ZnONPs. Biochemistry and Biophysics Reports. 2018; 14: 69–77.
[31] Sulaiman CT, Balachandran I. LC/MS characterization of phenolic antioxidants of Brindle berry (Garcinia gummi-gutta (L.) Robson). Natural Product Research. 2017; 31: 1191–1194.
[32] Jena BS, Jayaprakasha GK, Singh RP, Sakariah KK. Chemistry and biochemistry of (-)-hydroxycitric acid from Garcinia. Journal of Agricultural and Food Chemistry. 2002; 50: 10–22.
[33] Anandalakshmi K, Venugobal J, Ramasamy V. Characterization of silver nanoparticles by green synthesis method using Pedalium murex leaf extract and their antibacterial activity. Applied Nanoscience. 2016; 6: 399–408.
[34] Bar H, Bhui DK, Sahoo GP, Sarkar P, Pyne S, Misra A. Green synthesis of silver nanoparticles using seed extract of Jatropha curcas. Colloids and Surfaces A: Physicochemical and Engineering Aspects. 2009; 348: 212–216.
[35] Ajitha B, Reddy YAK, Reddy PS. Biogenic nano-scale silver particles by Tephrosia purpurea leaf extract and their inborn antimicrobial activity. Spectrochimica Acta. Part A, Molecular and Biomolecular Spectroscopy. 2014; 121: 164–172.
[36] Jiang J, Oberdörster G, Biswas P. Characterization of size, surface charge, and agglomeration state of nanoparticle dispersions for toxicological studies. Journal of Nanoparticle Research. 2009; 11: 77–89.
[37] Sharifi-Rad M, Anil Kumar NV, Zucca P, Varoni EM, Dini L, Panzarini E, *et al*. Lifestyle, Oxidative Stress, and Antioxidants: Back and Forth in the Pathophysiology of Chronic Diseases. Frontiers in Physiology. 2020; 11: 694.
[38] Saadat N, Gupta SV. Potential role of garcinol as an anticancer agent. Journal of Oncology. 2012; 2012: 647206.
[39] Liu C, Ho PCL, Wong FC, Sethi G, Wang LZ, Goh BC. Garcinol: Current status of its anti-oxidative, anti-inflammatory and anti-cancer effects. Cancer Letters. 2015; 362: 8–14.
[40] Saharan P, Chaudhary GR, Mehta SK, Umar A. Efficient photo-

catalytic degradation of victoria blue R and fast green FCF dyes using γ-Fe2O3 and Fe3O4 nanoparticles. Nanoscience and Nanotechnology Letters. 2016; 8: 965–971.
[41] Wei D, Ye Y, Jia X, Yuan C, Qian W. Chitosan as an active support for assembly of metal nanoparticles and application of the resultant bioconjugates in catalysis. Carbohydrate Research. 2010; 345: 74–81.
[42] He H, Yang S, Yu K, Ju Y, Sun C, Wang L. Microwave induced catalytic degradation of crystal violet in nano-nickel dioxide suspensions. Journal of Hazardous Materials. 2010; 173: 393–400.